

# Diffusion-Prepared Segmented Steady-State Free Precession: Application to 3D Black-Blood Cardiovascular Magnetic Resonance of the Thoracic Aorta and Carotid Artery Walls

Ioannis Koktzoglou, MS,<sup>1,2</sup> and Debiao Li, PhD<sup>1,2</sup>

Department of Radiology, Northwestern University, Chicago, Illinois, USA<sup>1</sup>

Department of Biomedical Engineering, Northwestern University, Evanston, Illinois, USA<sup>2</sup>

## ABSTRACT

This work developed a three-dimensional (3D) diffusion-prepared segmented steady-state free precession (DP-SSFP) cardiovascular magnetic resonance (CMR) sequence for black-blood (BB) thoracic aortic and carotid wall visualization. In 14 healthy volunteers, BB CMR of the thoracic aorta ( $n = 7$ ) and carotid arteries ( $n = 7$ ) was performed over 12 cm and 3 cm of transversal coverage, respectively, with a single 3D DP-SSFP acquisition and multiple two-dimensional (2D) slices using a T2-weighted (T2W) double inversion-recovery fast spin-echo (DIR-FSE) sequence. Arterial wall area (WA), lumen area (LA), and wall-lumen contrast-to-noise ratio (CNR) measured from the 3D DP-SSFP images were compared to those measured from the 2D T2W DIR-FSE images. Strong agreement in WA and LA between the two techniques was observed in the thoracic aorta (WA: intraclass correlation coefficient (ICC) = 0.866, LA: ICC = 0.993;  $p < 0.001$  for both) and carotid arteries (WA: ICC = 0.939, LA: ICC = 0.991;  $p < 0.001$  for both). Adjusted for slice thickness and number of slices, higher effective CNR per unit time (i.e., CNR efficiency) was attained with 3D DP-SSFP than 2D T2W DIR-FSE during thoracic aortic wall imaging ( $11.6 \pm 1.4$  vs.  $2.9 \pm 0.5$ ;  $p < 0.001$ ) and carotid artery wall imaging ( $10.1 \pm 1.9$  vs.  $3.1 \pm 0.5$ ;  $p < 0.001$ ). Diffusion-prepared segmented SSFP is a promising vessel wall CMR sequence that allows for 3D acquisition of thin and contiguous slices with BB image contrast.

## INTRODUCTION

Cardiovascular magnetic resonance (CMR) sequences that attenuate the signal from flowing blood are useful for depicting arterial anatomy since they yield good arterial wall conspicuity and contrast-to-noise ratio (CNR) between the arterial wall and lumen. These “black-blood” (BB) sequences, consisting of blood-attenuating magnetization preparations preceding fast spin-echo (FSE) image acquisitions (1–6), have been valuable in the non-invasive CMR assessment of atherosclerosis, a

progressive fibroproliferative and inflammatory disease that can cause cardiovascular events including myocardial and cerebral infarction (7, 8).

Two magnetization preparations typically used to attenuate the CMR signal from flowing blood are double inversion-recovery (DIR) (9, 10) and saturation band (SAT) (2, 11). In order to achieve BB image contrast with the DIR and SAT magnetization preparations, complete inflow of tagged (either inverted or saturated) blood spins into the imaged slice is necessary. Although these BB preparations effectively provide for blood-suppressed CMR of two-dimensional (2D) slices, three-dimensional (3D) BB CMR with DIR or SAT is difficult to achieve since complete inflow of tagged blood into the entire extent of arterial vasculature contained within the thick 3D imaging slab may not be possible. Three-dimensional BB CMR vessel wall imaging, however, is potentially advantageous over 2D BB CMR vessel wall imaging in respect to achievable signal-to-noise ratio, anatomical coverage, and spatial resolution.

Received 6 March 2006; accepted 28 May 2006.

Keywords: Vessel Wall Imaging, Thoracic Aorta, Carotid Arteries, Black-Blood Imaging.

Correspondence to:

Ioannis Koktzoglou

email: ioannis.koktzoglou@gmail.com

In the present work, a diffusion-prepared segmented steady-state free precession (DP-SSFP) imaging sequence is presented that allows for BB CMR of arterial wall morphology in 3D. A driven equilibrium Fourier transform (DEFT) diffusion preparation is used in the 3D DP-SSFP sequence to dephase moving blood spins to achieve BB image contrast (12, 13), without necessitating complete inflow of blood for BB effect as required by DIR and SAT. Segmented SSFP image acquisition is used to allow for signal-to-noise ratio-efficient imaging of the arterial wall in a time-efficient manner.

This study sought to investigate the 3D DP-SSFP sequence for 3D BB CMR of the thoracic aorta and the carotid arteries in healthy volunteers. T2-weighted (T2W) DIR-prepared FSE CMR, a conventional method for BB visualization of the aortic and carotid artery walls, was performed to provide a standard of reference. The arterial wall-lumen contrast-to-noise ratio (CNR), wall area, and lumen area measured from the 3D DP-SSFP images were compared to values obtained from the 2D T2W DIR-FSE images.

## MATERIALS AND METHODS

### Subjects

This HIPAA-compliant study was approved by our university's institutional review board. A total of 14 healthy volunteers were involved in this study. Written informed consent was obtained from all volunteers before CMR was performed. Thoracic aortic wall CMR was performed in 7 volunteers (7 males, mean age =  $40.6 \pm 11.9$  years, mean weight =  $81.4 \pm 10.3$  kg). Seven more volunteers (7 males, mean age =  $41.4 \pm 10.8$  years, mean weight =  $77.8 \pm 11.6$  kg) underwent CMR of the carotid arteries.

### CMR system

All CMR experiments were performed on a 1.5 T whole-body scanner (MAGNETOM Sonata, Siemens Medical Solutions, Erlangen, Germany) equipped with high-speed gradients (maximum gradient amplitude: 40 mT/m, maximum slew rate: 200 mT/m/ms). The scanner's body coil was used in all experiments for  $B_1$  field transmission. Two 6-element cardiac phased-array surface coils (Siemens Medical Solutions, Erlangen, Germany; coil size = 22 cm  $\times$  24 cm) were used for signal reception during aortic CMR, with one coil placed anterior and the other placed posterior to the thorax. Two 2-element carotid phased-array surface coils (Machnet BV, Elde, The Netherlands; coil size = 6 cm  $\times$  12 cm) were used for signal reception during carotid CMR, with one coil placed on the left and the other placed on the right side of the neck.

### Sequence structure

A diffusion-prepared segmented 3D steady-state free precession sequence was constructed to allow for 3D dark-blood

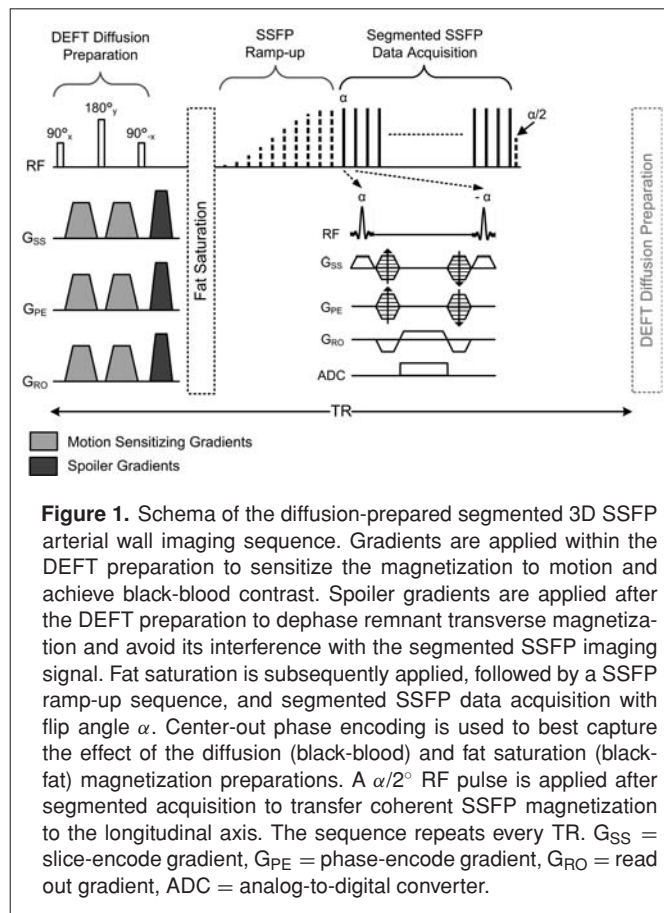


**Figure 1.** Schema of the diffusion-prepared segmented 3D SSFP arterial wall imaging sequence. Gradients are applied within the DEFT preparation to sensitize the magnetization to motion and achieve black-blood contrast. Spoiler gradients are applied after the DEFT preparation to dephase remnant transverse magnetization and avoid its interference with the segmented SSFP imaging signal. Fat saturation is subsequently applied, followed by a SSFP ramp-up sequence, and segmented SSFP data acquisition with flip angle  $\alpha$ . Center-out phase encoding is used to best capture the effect of the diffusion (black-blood) and fat saturation (black-fat) magnetization preparations. A  $\alpha/2^\circ$  RF pulse is applied after segmented acquisition to transfer coherent SSFP magnetization to the longitudinal axis. The sequence repeats every TR.  $G_{SS}$  = slice-encode gradient,  $G_{PE}$  = phase-encode gradient,  $G_{RO}$  = read out gradient, ADC = analog-to-digital converter.

vessel wall CMR. As shown in Figure 1, diffusion sensitization was imparted by a  $90_x^\circ-180_y^\circ-90_x^\circ$  DEFT sequence containing spatially non-selective, “hard” radiofrequency (RF) pulses and interspersed with empirically determined magnetic field gradients in the readout, phase encoding, and slice directions (14–17). Diffusion sensitization was used to dephase moving blood spins in order to achieve dark-blood appearance (12, 13). Spoiler gradients were applied after the conclusion of the DEFT preparation to spoil remnant transverse magnetization.

The DEFT diffusion preparation was followed by a chemically-selective fat saturation RF pulse to suppress signal from perivascular fat and improve the conspicuity of the arterial wall. Ten sinusoidally-modulated SSFP ramp-up RF pulses were applied before segmented SSFP data acquisition to ensure a smooth signal evolution and to minimize image artifacts during data acquisition (18). Centric (i.e., low-high) phase-encode ordering was used during SSFP acquisition to place greatest diffusion weighting at the center of k-space (14, 16), allowing for black-blood imaging. Linear k-space ordering was used in the slice-encoding direction.

### Aortic CMR

Volunteers were instructed to breathe normally during the CMR procedure. In each volunteer the thoracic aorta was

localized through acquisition of transverse, coronal, and sagittal electrocardiographically (ECG)-triggered segmented SSFP scout images.

Based on these scout images, a 12-cm-thick axially-oriented 3D DP-SSFP imaging slab was prescribed containing the ascending aorta, the aortic arch, and a portion of the descending thoracic aorta. ECG triggering was used during 3D DP-SSFP imaging with data acquisition performed during diastole. Typical aortic imaging sequence parameters with 3D DP-SSFP were: repetition time (TR) = 1 R to R interval (R-R), field-of-view (FOV) = 27.5 (readout)  $\times$  20.6 (phase) cm<sup>2</sup>, matrix = 256  $\times$  192 (yielding 1.07  $\times$  1.07 mm<sup>2</sup> in-plane spatial resolution), 53-71 segments per TR, imaging bandwidth (BW) = 1220 Hz/pixel, segment TR/echo time (TE) = 3.8/1.9 ms, flip angle ( $\alpha$ ) = 45°, 48 slices, slice thickness (SL<sub>TH</sub>) = 2.5 mm, slice oversampling (SO) = 17%, averages (NEX) = 3. The duration of the magnetic field gradients applied before and after the 180° RF pulse within the DEFT preparation was 2.1  $\pm$  0.2 ms. Total gradient areas applied within the DEFT diffusion preparation in the readout, phase encoding, and slice directions (in units of ms $\cdot$ mT $\cdot$ m<sup>-1</sup>) were 12.1  $\pm$  11.5, 12.1  $\pm$  11.5, and 115.5  $\pm$  27.4, respectively, corresponding to a cumulative b-value of 0.7  $\pm$  0.4 s/mm<sup>2</sup>. The rationale for imparting stronger diffusion sensitization in the slice direction was to most effectively suppress the appearance of axially-moving aortic blood flow, the predominant blood flow direction in the thoracic aorta (19, 20).

To provide a standard of reference for assessing the 3D DP-SSFP images, conventional dark-blood CMR of the aorta was performed with an ECG-triggered T2-weighted 2D DIR-FSE sequence. Within the same 12 cm thick volume imaged with 3D DP-SSFP, 12–24 evenly-spaced transverse 2D DIR-FSE slices were acquired sequentially. The 2D DIR-FSE images were matched in terms of spatial resolution (1.07  $\times$  1.07 mm<sup>2</sup>) with the 3D DP-SSFP images in both the readout and phase encoding directions (FOV = 27.5  $\times$  20.6 cm<sup>2</sup>, matrix = 256  $\times$  192). Remaining imaging parameters for the 2D DIR-FSE sequence were matched to literature values (21): free-breathing acquisition, chemically-selective fat saturation, TR = 2 R-R, TE = 59 ms, echo train length (ETL) = 33, BW = 490 Hz/pixel, echo spacing (ES) = 5.5 ms,  $\alpha$  = 180°, SL<sub>TH</sub> = 5 mm, NEX = 2.

### ***Carotid CMR***

Volunteers were instructed to abstain from swallowing during the CMR procedure. The carotid bifurcations of each volunteer were localized on axial and oblique-sagittal segmented SSFP scout images.

Based on the localizer images, a 3-cm-thick axially-oriented 3D DP-SSFP imaging slab was prescribed containing both carotid bifurcations. ECG triggering was not used in accordance to the findings of Mani et al. (22). Typical carotid imaging sequence parameters with 3D DP-SSFP were: TR = 1 sec, FOV = 12  $\times$  12 cm<sup>2</sup>, matrix = 256  $\times$  256 (yielding 0.47  $\times$  0.47 mm<sup>2</sup> in-plane spatial resolution), 65 segments per TR, BW = 560 Hz/pixel, segment TR/TE = 5.8/2.9 ms,  $\alpha$  = 45°,

20 slices (interpolated to 30), SL<sub>TH</sub> = 1.5 mm (interpolated to 1.0 mm), SO = 20%, NEX = 2, TA = 192 s. The duration of the magnetic field gradients applied before and after the 180° RF pulse within the DEFT preparation was 3.9  $\pm$  0.4 ms. Total gradient area applied along each direction (readout, phase encoding, slice) was 231.4  $\pm$  22.7 ms $\cdot$ mT $\cdot$ m<sup>-1</sup>, corresponding to a cumulative b-value of 11.1  $\pm$  2.4 s/mm<sup>2</sup>. Complex, multi-directional blood flow is known to reside in internal carotid artery bulb (23,24). To eliminate signal from moving blood involved in these flow patterns, equal amounts of diffusion sensitization were applied in the readout, phase encoding, and slice directions.

Conventional ECG-triggered T2-weighted 2D DIR-FSE carotid vessel wall imaging was performed for comparison with 3D DP-SSFP. Within the 3 cm thick volume imaged with 3D DP-SSFP, 5 evenly-spaced transverse 2D DIR-FSE slices were acquired sequentially. The 2D DIR-FSE images were matched in terms of spatial resolution (0.47  $\times$  0.47 mm<sup>2</sup>) with the 3D DP-SSFP images in both the readout and phase encoding directions (FOV = 12  $\times$  12 cm<sup>2</sup>, matrix = 256  $\times$  256). Remaining 2D DIR-FSE imaging parameters were matched to literature values (1): chemically-selective fat saturation, TR = 3 R-R, TE = 50 ms, ETL = 13, BW = 190 Hz/pixel, ES = 10 ms,  $\alpha$  = 180°, SL<sub>TH</sub> = 2 mm, NEX = 2.

### ***Image analysis***

Images were transferred from the CMR scanner to a personal computer loaded with ImageJ (version 1.34s, National Institutes of Health, Bethesda, MD, USA) for signal and morphometric analysis by an author with 3 years CMR experience.

### ***Signal analysis***

In each pair of DP-SSFP and DIR-FSE images located at the same axial position, signal measurements of air, arterial wall, and arterial lumen were taken. In cases where the axial positions of the images slightly differed due to differences in slice thickness, the closest sets of images were used. Bulk patient motion between imaging sequences was assessed through visual inspection and compensated for by registering anatomic landmarks outside of the artery of interest.

First, noise was measured as the standard deviation of air signal ( $\sigma_N$ ) enclosed within manually-drawn regions-of-interest (ROI) no smaller than 100 mm<sup>2</sup> and 25 mm<sup>2</sup> in the aortic and carotid images, respectively. Images were subsequently bilinearly interpolated by a factor of 5 for further analysis. Arterial wall signal ( $S_W$ ) was measured as the average value of a pixel path (path width = 1 pixel) manually drawn to outline the arterial wall. Arterial lumen signal ( $S_L$ ) was measured as the mean signal contained within a ROI drawn in the arterial lumen.

Wall-lumen contrast-to-noise ratio (CNR) was calculated by the relation  $(S_W - S_L) / \sigma_N$ . CNR values were averaged to yield one CNR value for each imaging sequence and volunteer. To

**Table 1.** Aortic imaging: CNR comparison between 3D DP-SSFP and 2D T2W DIR-FSE

Subject	Imaging Time (s) [number of imaging slices] (slice thickness in mm)		Wall-Lumen CNR		Wall-Lumen CNR <sub>eff</sub>	
	3D DP-SSFP	2D T2W DIR-FSE	3D DP-SSFP	2D T2W DIR-FSE	3D DP-SSFP	2D T2W DIR-FSE
A	589 [48] (2.5)	316 [12] (5)	12.0	8.2	10.6	2.5
B	380 [48] (2.5)	206 [12] (5)	9.6	10.4	10.6	3.9
C	606 [48] (2.5)	645 [24] (5)	14.5	8.8	12.6	2.2
D	447 [48] (2.5)	537 [24] (5)	9.4	8.5	9.6	2.8
E	379 [48] (2.5)	493 [24] (5)	12.0	7.7	13.3	2.6
F	480 [48] (2.5)	616 [24] (5)	13.3	8.2	13.2	2.5
G	454 [48] (2.5)	457 [24] (5)	11.1	9.6	11.2	3.4
Mean ± SD	9.9 ± 1.9 sec/slice	22.6 ± 3.8 sec/slice	11.7 ± 1.9	8.8 ± 0.9	11.6 ± 1.4	2.9 ± 0.5
p value	< 0.001		0.018		< 0.001	

allow for fair comparison of CNR values with respect to imaging parameter differences, CNR efficiency (CNR<sub>eff</sub>) was calculated by the relation, adapted from references (6, 25):

$$\text{CNR}_{\text{eff}} = \frac{\text{CNR}\sqrt{N}}{\text{SL}_{\text{TH}}\sqrt{\text{TA}}} = \frac{\text{CNR}}{\text{SL}_{\text{TH}}\sqrt{\text{TA}_{\text{SLICE}}}}, \quad [1]$$

where N is the number of imaging slices, SL<sub>TH</sub> is the imaging slice thickness (in millimeters), TA is the total imaging time (in minutes), and TA<sub>SLICE</sub> is the imaging time per slice (in minutes). Adjustment of CNR by SL<sub>TH</sub> rather than voxel volume was fair since both sequences had equal in-plane spatial resolutions.

### Morphometric analysis

In each pair of DP-SSFP and DIR-FSE images located at the same axial position, paths were manually drawn to outline the inner and outer boundaries of the arterial wall. The coordinates of the arterial wall boundaries (expressed in millimeters) were exported from ImageJ and subsequently loaded into Matlab (version 7.0, The Mathworks, Inc., Natick, Massachusetts, USA) for automatic calculation of arterial lumen area and wall area.

### Statistical analysis

Statistical analysis was performed in SPSS (v11.0, SPSS Inc., Chicago, Illinois, USA). For both aortic and carotid CMR, two-tailed matched-paired *t*-tests were performed on CNR and CNR<sub>eff</sub> to determine whether values differed between 3D DP-SSFP and 2D DIR-FSE. Comparison of the time each sequence took to acquire one imaging slice was performed through two-tailed matched-paired *t*-tests. Agreement of lumen area and wall area measurements between imaging sequences was assessed through calculation of intraclass correlation coefficient (ICC), linear regression, and the method of Bland and Altman (26). In all tests, statistical significance was defined at the *p* < 0.05 level.

## RESULTS

### Aortic CMR

Measured wall-lumen CNR and computed CNR<sub>eff</sub> values obtained during aortic CMR are listed in Table 1. Statistically significant differences in wall-lumen CNR between 3D DP-SSFP and 2D T2W DIR-FSE were detected (11.7 ± 1.9 vs. 8.8 ± 0.9, respectively; *p* = 0.018), with DP-SSFP values observed to be larger. Wall-lumen CNR<sub>eff</sub> was significantly higher with 3D DP-SSFP than with 2D T2W DIR-FSE (11.6 ± 1.4 vs. 2.9 ± 0.5, respectively; *p* < 0.001). Imaging time per section with 3D DP-SSFP was 44% of the imaging time per section associated with 2D DIR-FSE (9.9 ± 1.9 sec vs. 22.6 ± 3.8 sec, respectively; *p* < 0.001).

Due to differences in acquisition window duration between imaging sequences, it was not always possible to trigger the 3D DP-SSFP sequence to begin at the same time point (post ECG R-wave) as the 2D T2W DIR-FSE sequence while fitting the acquisition window before the onset of the next R-wave. Mean trigger times (post ECG R-wave) for the 3D DP-SSFP and 2D T2W DIR-FSE sequences therefore differed, and were 523 ± 159 ms and 640 ± 62 ms, respectively (paired *t*-test; *p* < 0.05).

Representative images of the thoracic aorta obtained with 3D DP-SSFP and 2D T2W DIR-FSE in a volunteer are shown in Figure 2. Delineation of the thoracic aortic wall with suppression of intra-luminal blood signal was observed with both imaging sequences. Morphometric measurements of aortic wall area (WA<sub>aorta</sub>) and aortic lumen area (LA<sub>aorta</sub>) made from the 3D DP-SSFP and 2D T2W DIR-FSE images were highly correlated (WA<sub>aorta</sub>: ICC = 0.866, linear regression *r* = 0.947, LA<sub>aorta</sub>: ICC = 0.993, linear regression *r* = 0.995; *p* < 0.001 for all). Scatter and Bland-Altman plots for aortic wall area and lumen area are shown in Figure 3. Measured WA<sub>aorta</sub> and LA<sub>aorta</sub> values from the 3D DP-SSFP images were, on average, 15.4% and 5.5% smaller than the average measurements made with both sequences. Relative to 2D T2W DIR-FSE measurements, significant negative bias (*r* = -0.190; *p* < 0.05) and positive bias (*r* = 0.272; *p* < 0.01) was present with 3D DP-SSFP measurements of WA<sub>aorta</sub> and LA<sub>aorta</sub>, respectively.

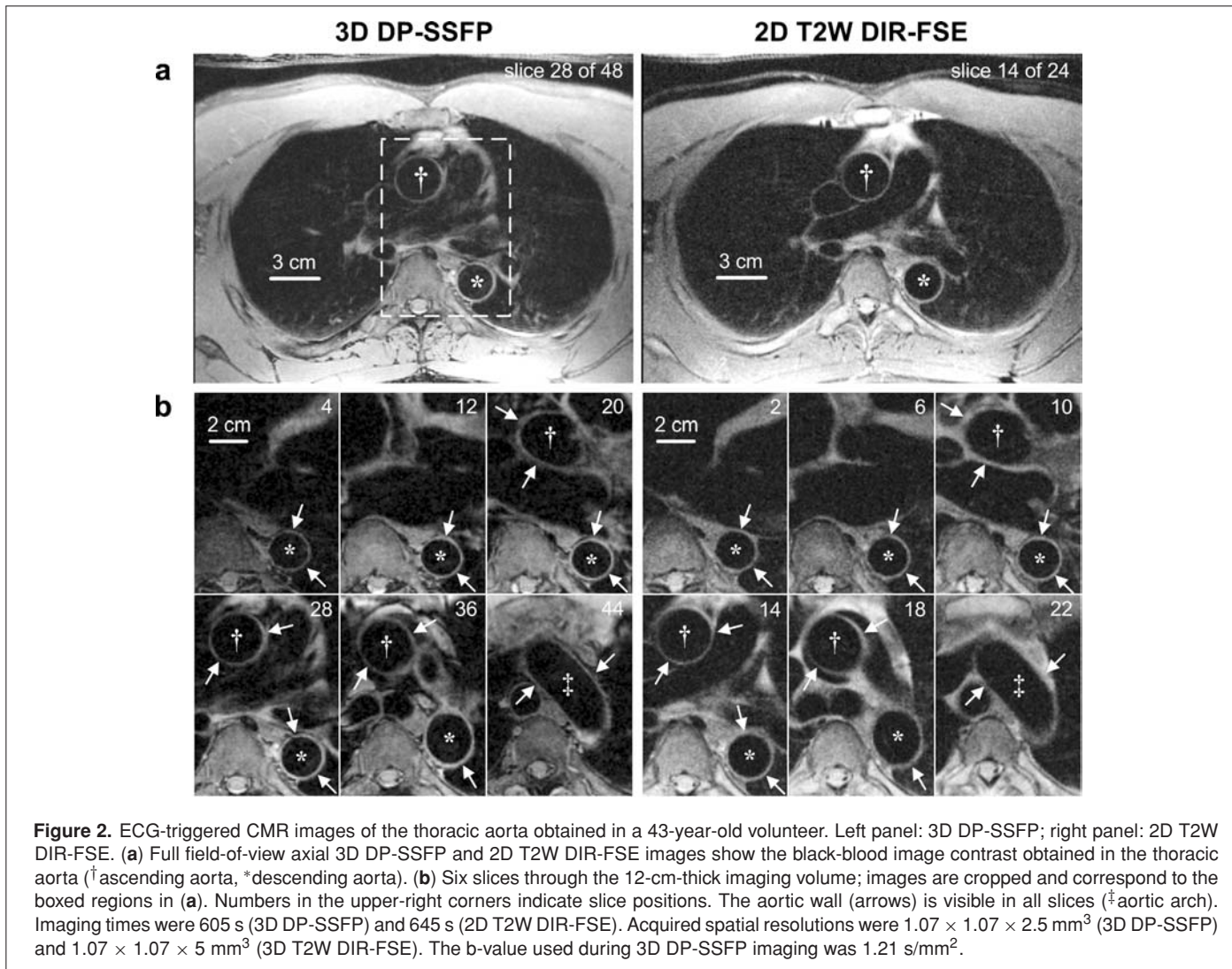


**Figure 2.** ECG-triggered CMR images of the thoracic aorta obtained in a 43-year-old volunteer. Left panel: 3D DP-SSFP; right panel: 2D T2W DIR-FSE. (a) Full field-of-view axial 3D DP-SSFP and 2D T2W DIR-FSE images show the black-blood image contrast obtained in the thoracic aorta († ascending aorta, \* descending aorta). (b) Six slices through the 12-cm-thick imaging volume; images are cropped and correspond to the boxed regions in (a). Numbers in the upper-right corners indicate slice positions. The aortic wall (arrows) is visible in all slices (‡ aortic arch). Imaging times were 605 s (3D DP-SSFP) and 645 s (2D T2W DIR-FSE). Acquired spatial resolutions were  $1.07 \times 1.07 \times 2.5 \text{ mm}^3$  (3D DP-SSFP) and  $1.07 \times 1.07 \times 5 \text{ mm}^3$  (3D T2W DIR-FSE). The b-value used during 3D DP-SSFP imaging was  $1.21 \text{ s/mm}^2$ .

### Carotid CMR

Measured wall-lumen CNR and computed  $\text{CNR}_{\text{eff}}$  values obtained during carotid CMR are listed in Table 2. Statistically significant differences in wall-lumen CNR between 3D DP-SSFP

and 2D T2W DIR-FSE were detected ( $6.0 \pm 1.1$  vs.  $7.5 \pm 1.2$ , respectively;  $p < 0.001$ ), with DIR-FSE values observed to be larger. Wall-lumen  $\text{CNR}_{\text{eff}}$  was significantly higher with 3D DP-SSFP than with 2D T2W DIR-FSE ( $10.1 \pm 1.9$  vs.  $3.1 \pm 0.5$ , respectively;  $p < 0.001$ ). Imaging time per section with 3D

**Table 2.** Carotid imaging: CNR comparison between 3D DP-SSFP and 2D T2W DIR-FSE

Subject	Imaging Time (s) [number of imaging slices] (slice thickness in mm)		Wall-Lumen CNR		Wall-Lumen $\text{CNR}_{\text{eff}}$	
	3D DP-SSFP	2D T2W DIR-FSE	3D DP-SSFP	2D T2W DIR-FSE	3D DP-SSFP	2D T2W DIR-FSE
H	192 [20] (1.5)	477 [5] (2)	6.5	8.7	10.9	3.4
I	192 [20] (1.5)	394 [5] (2)	7.7	8.8	12.9	3.8
J	192 [20] (1.5)	515 [5] (2)	6.0	7.7	10.0	2.9
K	192 [20] (1.5)	390 [5] (2)	7.0	7.8	11.7	3.4
L	192 [20] (1.5)	404 [5] (2)	4.6	5.2	7.7	2.2
M	192 [20] (1.5)	416 [5] (2)	5.3	7.1	9.0	3.0
N	192 [20] (1.5)	450 [5] (2)	4.9	6.9	8.2	2.8
Mean $\pm$ SD	$9.6 \pm 0.0$ sec/slice	$87.0 \pm 9.5$ sec/slice	$6.0 \pm 1.1$	$7.5 \pm 1.2$	$10.1 \pm 1.9$	$3.1 \pm 0.5$
p value	<0.001		<0.001		<0.001	

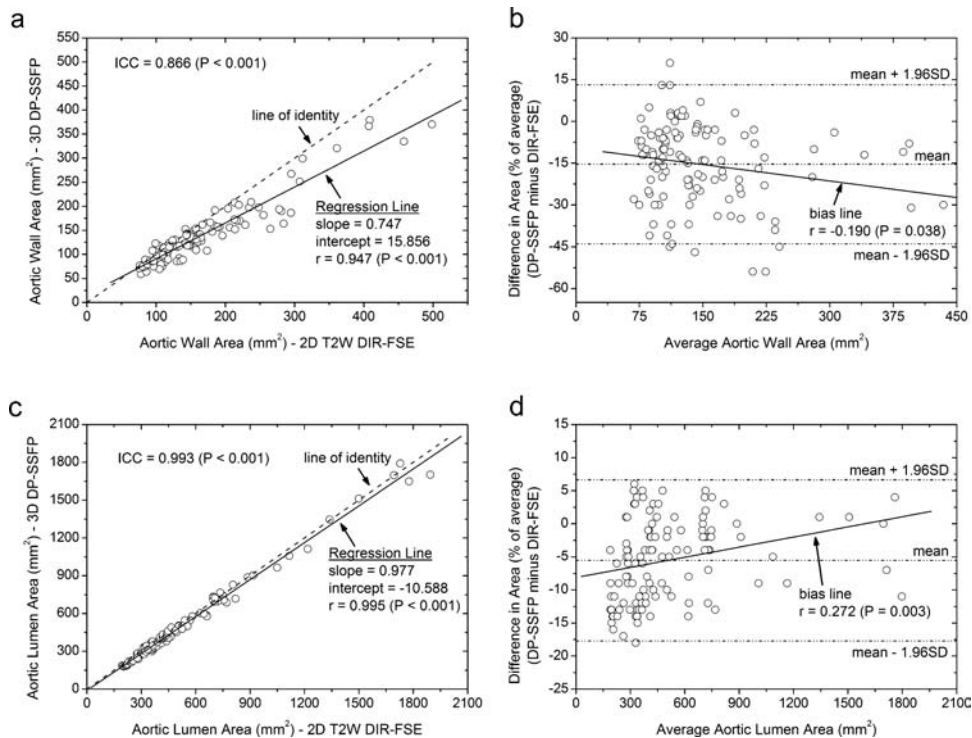


**Figure 3.** (a) Scatter plot of aortic wall area as measured from the 3D DP-SSFP and 2D T2W DIR-FSE images (ICC = 0.866, linear regression  $r = 0.947$ ;  $p < 0.001$  for both). (b) Bland-Altman plot of percentage difference in aortic wall area versus average aortic wall area showing the limits of agreement. (c) Scatter plot of aortic lumen area as measured from both sequences (ICC = 0.993, linear regression  $r = 0.995$ ;  $p < 0.001$  for both). (d) Bland-Altman plot of percentage difference in aortic lumen area versus average aortic lumen area showing the limits of agreement.

DP-SSFP was 11% of the imaging time per section associated with 2D DIR-FSE (9.6 s vs.  $87.0 \pm 9.5$  s, respectively;  $p < 0.001$ ).

Representative images of the carotid arteries obtained with 3D DP-SSFP and 2D T2W DIR-FSE in a volunteer are shown in Figure 4. Delineation of the carotid artery wall with suppression of intra-luminal blood signal was observed with both imaging sequences. Morphometric measurements of carotid wall area ( $WA_{\text{carotid}}$ ) and carotid lumen area ( $LA_{\text{carotid}}$ ) made from the 3D DP-SSFP and 2D T2W DIR-FSE images were highly correlated ( $WA_{\text{carotid}}$ : ICC = 0.939, linear regression  $r = 0.945$ ,  $LA_{\text{carotid}}$ : ICC = 0.991, linear regression  $r = 0.992$ ;  $p < 0.001$  for all). Scatter and Bland-Altman plots of carotid wall area and lumen area are shown in Figure 5. Measured  $WA_{\text{carotid}}$  and  $LA_{\text{carotid}}$  values from the 3D DP-SSFP images were, on average, 7.6% and 4.7% smaller than the average measurements made with both sequences. Bias was not present between measurements of  $WA_{\text{carotid}}$  ( $r = 0.141$ ;  $p > 0.05$ ) and  $LA_{\text{carotid}}$  ( $r = -0.190$ ;  $p > 0.05$ ).

## DISCUSSION

In this work, a fat-saturated segmented diffusion-prepared SSFP sequence was developed for 3D black-blood CMR of the thoracic aorta and carotid arteries. Good agreement of arterial wall and lumen areas measured from the 3D DP-SSFP and 2D

T2W DIR-FSE images was found for aortic and carotid artery wall imaging. Two-dimensional T2W DIR-FSE was selected for comparison because it is the most commonly used technique for vessel wall imaging at the present time.

During aortic imaging, however,  $WA_{\text{aorta}}$  values from the 2D T2W DIR-FSE images were larger than those from the 3D DP-SSFP images. A significant bias was also detected during Bland-Altman analysis, with 3D DP-SSFP underestimating  $WA_{\text{aorta}}$  and overestimating  $LA_{\text{aorta}}$  (relative to 2D T2W DIR-FSE) for large measurements, which, from our observation, often occurred in the aortic arch. A possible reason for both of these findings may have been the increased partial volume averaging with DIR-FSE imaging, especially in the aortic arch, resulting from acquisition of thicker slices (5 mm vs. 2.5 mm, 2D T2W DIR-FSE vs. 3D DP-SSFP). It is also possible that the use of a long FSE acquisition window during aortic imaging (33 echoes  $\times$  5.5 ms/echo = 181.5 ms) may have resulted in image blurring of the 2D T2W DIR-FSE images. Image blurring is known to occur in FSE sequences with echo train duration much longer than tissue T2 (27). Better agreement of wall area among sequences was observed during carotid CMR, possibly due to closely-matched slice spatial resolutions (2 mm vs. 1.5 mm, 2D T2W DIR-FSE vs. 3D DP-SSFP) and use of a shorter FSE acquisition window (13 echoes  $\times$  10 ms/echo = 130 ms).

Wall-lumen  $CNR_{\text{eff}}$  values obtained with segmented 3D DP-SSFP during both aortic and carotid CMR were significantly

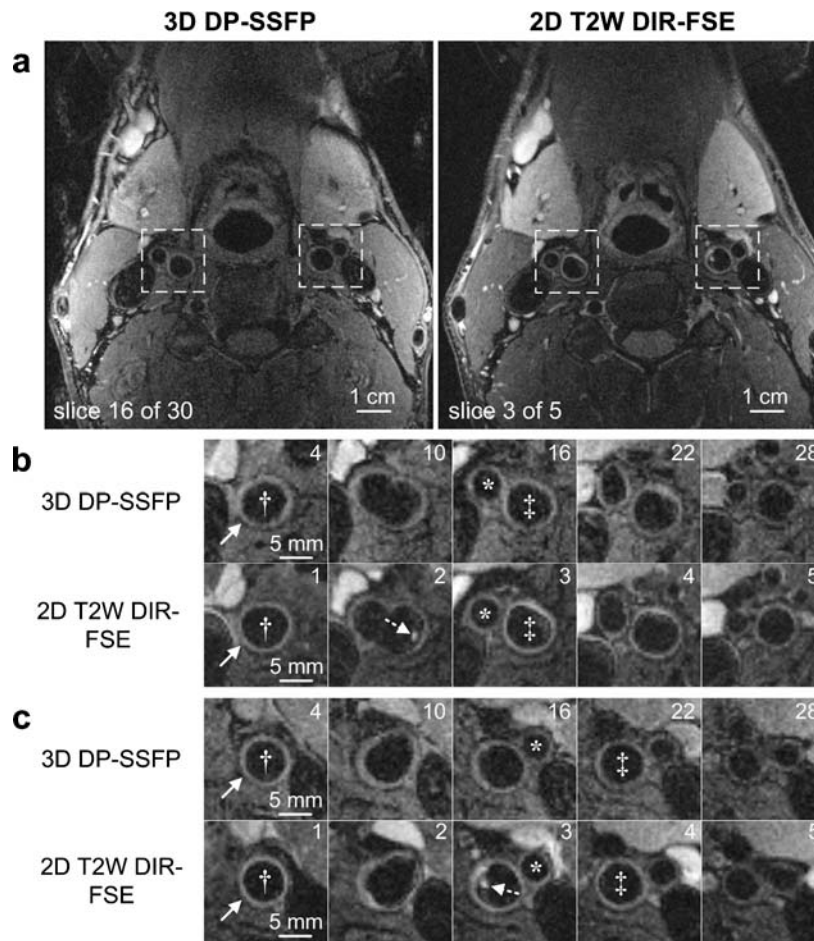


**Figure 4.** (a) Transverse full field-of-view 3D DP-SSFP and ECG-triggered 2D T2W DIR-FSE images through the neck obtained in a 50-year-old volunteer. Transverse images depicting the right (b) and left (c) carotid arteries (†common carotid, ‡internal carotid, \*external carotid); images magnified and correspond to the boxed regions in a. Numbers in the upper-right corners indicate slice positions. Note the similar depiction of the carotid arterial wall (solid arrows) with both imaging sequences. In this volunteer, residual blood signal was observed in the internal carotid arterial lumen in the 2D T2W DIR-FSE images (dashed arrows) but not in the 3D DP-SSFP images. Imaging times were 192 s (3D DP-SSFP; 20 acquired (interpolated to 30) slices) and 394 s (2D T2W DIR-FSE; 5 slices). Acquired spatial resolutions were  $0.47 \times 0.47 \times 1.5 \text{ mm}^3$  (3D DP-SSFP) and  $0.47 \times 0.47 \times 2 \text{ mm}^3$  (3D T2W DIR-FSE). The b-value used during 3D DP-SSFP imaging was  $11.97 \text{ s/mm}^2$ .

higher than the  $\text{CNR}_{\text{eff}}$  obtained with 2D T2W DIR-FSE. In the aortic imaging studies, 3D DP-SSFP achieved, on average, 1.33 times the CNR, 50% of the voxel volume, and 44% of the imaging time per slice of 2D DIR-FSE. This resulted in a 4-fold improvement of  $\text{CNR}_{\text{eff}}$  with 3D DP-SSFP over 2D DIR-FSE. In the carotid CMR studies, 3D DP-SSFP achieved, on average, 80% the CNR of 2D T2W DIR-FSE with 25% reduced voxel volume and 11% of the imaging time per slice required by 2D DIR-FSE. This led to a 3.25-fold improvement in  $\text{CNR}_{\text{eff}}$  with 3D DP-SSFP over 2D DIR-FSE.

The versatility of the segmented 3D DP-SSFP imaging sequence for BB vessel wall imaging was demonstrated through imaging of the thoracic aorta and the carotid arteries, two vessels often afflicted with atherosclerosis (28–30). CMR of the thoracic aorta with 3D DP-SSFP demonstrated the sequence's ability for imaging of a thick volume containing tortuous ar-

terial morphology (i.e., the aortic arch) in 3D with BB image contrast, a non-trivial feat with conventional inflow-based black-blood preparation methods (e.g., double inversion-recovery and saturation band). Furthermore, based on the non-selective nature of the DEFT diffusion preparation, it is expected that 3D DP-SSFP should also allow for BB imaging with slab orientations oblique or parallel to the long axis of the artery being imaged. The carotid CMR performed in this study demonstrated 3D DP-SSFP's ability for high spatial resolution BB arterial wall imaging of a small, localized anatomical region. Importantly, plaque-mimicking flow artifacts previously observed and described in the internal carotid artery bulb during BB CMR (2) were not present in the 3D DP-SSFP images. These flow artifacts, however, were sometimes seen in the 2D DIR-FSE images. For in-slice or slow flow, it is possible that the phase dispersion imparted by the diffusion preparation may have been sufficient to produce a signal void, while the time-of-flight

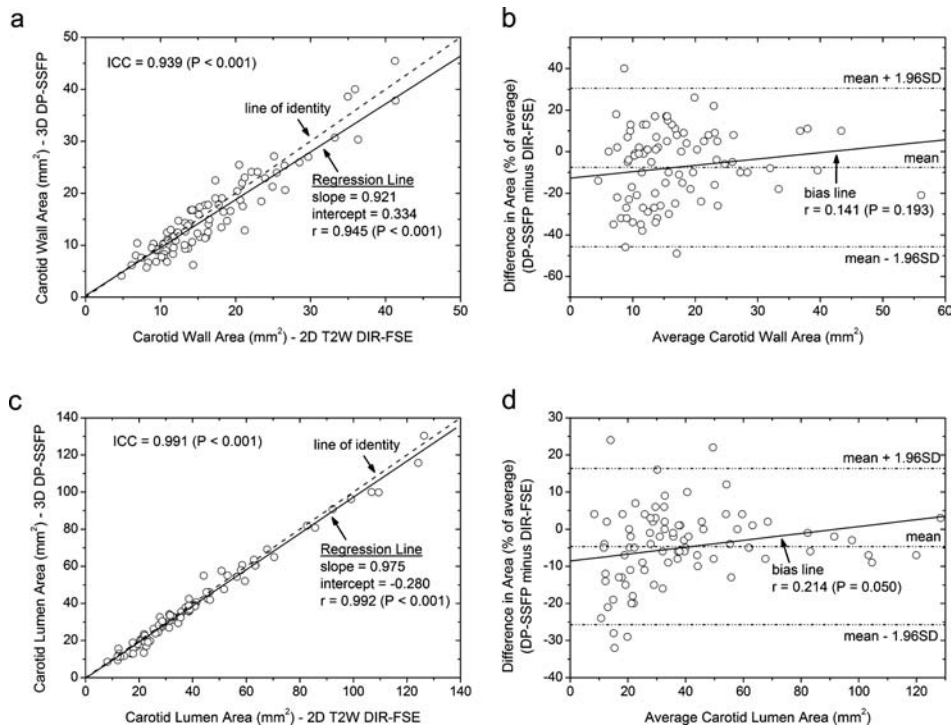


**Figure 5.** (a) Scatter plot of carotid wall area as measured from the 3D DP-SSFP and 2D T2W DIR-FSE images (ICC = 0.939, linear regression  $r = 0.945$ ;  $p < 0.001$  for both). (b) Bland-Altman plot of percentage difference in carotid wall area versus average carotid wall area showing the limits of agreement. (c) Scatter plot of carotid lumen area as measured from both sequences (ICC = 0.991, linear regression  $r = 0.992$ ;  $p < 0.001$  for both). (d) Bland-Altman plot of percentage difference in carotid lumen area versus average carotid lumen area showing the limits of agreement.

condition needed by 2D DIR-FSE for BB appearance may not have been met.

The 3D DP-SSFP CMR sequence produced thin and contiguous slices that, after multi-planar reconstruction, allowed for

in-plane visualization of both the aortic and carotid walls along arbitrary imaging planes (Fig. 6). Clearly, CMR with isotropic spatial resolution rather than with slice thickness greater than the in-plane pixel dimensions, as performed in this study, would

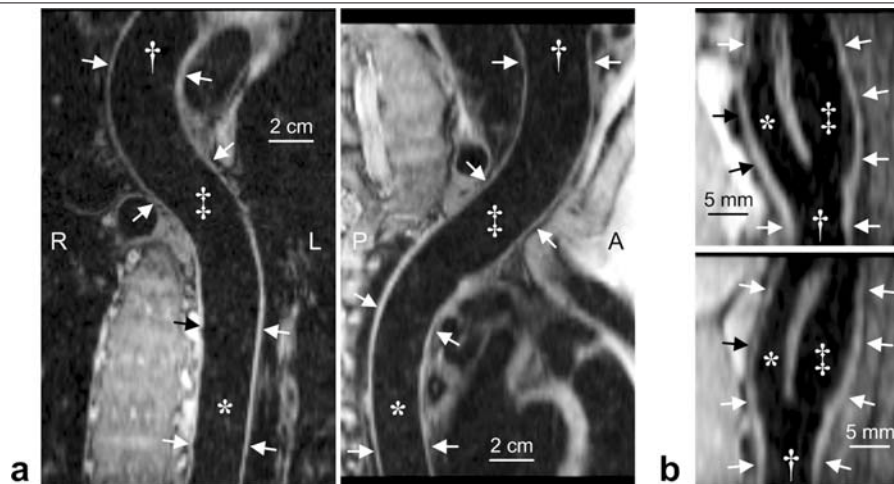


**Figure 6.** (a) Left panel: Coronal curved MPR from the aortic 3D DP-SSFP data set shown in Figure 2. Right panel: Sagittal curved MPR from the same data set. Note the conspicuity of the aortic wall (arrows) throughout the length of the thoracic aorta († ascending aorta, ‡ aortic arch, \* descending aorta) in both reformations. (b) MPRs from the 3D DP-SSFP data set shown in Figure 4 displaying the right (top panel) and left (bottom panel) carotid artery bifurcations († common carotid, ‡ internal carotid, \* external carotid). Note the conspicuity of the carotid arterial wall (arrows) proximal and distal to the bifurcation.

have been better for multi-planar reconstruction. In patients with atherosclerosis, thin and contiguous slices could be useful for estimating total plaque burden (in the aorta, for example). Previous studies in patients examining aortic wall dimensions have used 2D DIR-FSE sequences with slice thicknesses of 4–5 mm—presumably to achieve acceptable wall-lumen CNR—and interslice gaps of 8–10 mm to allow for anatomical coverage of the region of interest given the imaging time limit (31,33). The proposed 3D DP-SSFP sequence which is capable of acquiring thin and contiguous slices could be a promising alternative to 2D DIR-FSE in future investigations of the aortic wall.

This study had certain limitations. First, the durations and amplitudes of the diffusion gradients (i.e. the b-values) within the 3D DP-SSFP sequence were empirically determined based on short, low-resolution preparatory scans in which BB image contrast was visually evaluated. Initial estimation of appropriate b-values producing sufficient blood signal suppression was performed in the first few volunteers imaged. In subsequent volunteers, these b-values were used as is, or were adjusted to improve the level of blood signal suppression without imparting too high of a b-value to unnecessarily reduce imaging signal-to-noise ratio (SNR). In preliminary work performed in our laboratory using segmented 3D DP-SSFP for carotid imaging, diffusion sensitization with a b-value of 12 s/mm<sup>2</sup> reduced the SNR of sternocleidomastoid muscle by 28% (72% of the SNR was retained) relative to an identical, but non-diffusion-prepared, segmented 3D SSFP sequence (data not shown). In the clinical setting, it would obviously be beneficial for the b-values to be fixed for all patients. The mean b-values used in this work could serve as starting points in the selection of these parameters.

Second, it would have been useful to verify arterial wall dimensions with a reference imaging procedure such as ultrasound, which is often used to measure intima-media thickness. Without such verification, it was not possible to determine whether one sequence was more accurate at measuring artery wall dimensions. Nonetheless, strong agreement of morphometric measurements between 3D DP-SSFP and 2D DIR-FSE measurements was observed in both the aorta and in the carotid arteries.

Third, it would have been useful to compare arterial wall dimensions and CNR efficiency of 3D DP-SSFP to those of multi-slice black-blood 2D DIR-FSE imaging sequences (3–6) which allow for acquisition of several slices in a single repetition time. In this work, comparison of 3D DP-SSFP was made with single-slice 2D DIR-FSE since the latter sequence is superior to multi-slice DIR methods in achieving BB image contrast, and single-slice 2D DIR-FSE has been documented in numerous patient studies. According to a previous report (6), CMR sequences that allow for simultaneous acquisition of up to 20 black-blood 2D DIR-FSE imaging sections could lead to a 2.5-fold improvement of CNR efficiency over single-slice acquisitions. Even with this improvement, the CNR efficiency of multi-slice 2D DIR-FSE would be lower than that of 3D DP-SSFP, according to our estimation. Obviously, a direct comparison of segmented

3D DP-SSFP to multi-slice DIR methods could be the topic of future work.

Fourth, a limitation of the 3D DP-SSFP sequence as presented here for aortic imaging was that 3 averages were acquired to mitigate respiratory artifacts. This led to larger than necessary scan times. We expect, however, that future implementations of segmented 3D DP-SSFP sequence could integrate navigator gating and saturation of the chest wall to remove respiratory motion artifacts and reduce scan times associated with aortic imaging.

A final limitation with this study is that all subjects imaged were healthy volunteers. Previous studies have reported that patients afflicted with atherosclerosis suffer from increased arterial stiffness and reduced arterial distensibility (34, 35). Given that diffusion sensitizing gradients are used during the 3D DP-SSFP imaging sequence to suppress signal from flowing blood, 3D DP-SSFP may better delineate less-mobile, atherosclerotic arterial walls. However, since blood flow velocities in the thoracic aorta appear to decrease with age (36), use of b-values higher than those used in this work with 3D DP-SSFP may be necessary to ensure black-blood image contrast in patient examinations of the thoracic aorta, possibly reducing imaging SNR. On the other hand, the high velocity blood flow jets found in patients with atherosclerotic carotid artery stenosis (37) may allow for use of lower b-values than used in this study during carotid imaging. Clearly, further investigation of the segmented 3D DP-SSFP CMR sequence in patients is needed to clarify these issues.

In conclusion, segmented 3D DP-SSFP is a fast and CNR-efficient sequence that allows for black-blood CMR of thoracic aortic and carotid arterial walls with thin and contiguous imaging slices. In healthy volunteers, strong agreement in arterial wall and lumen areas in the thoracic aorta and carotid arteries was made with 3D DP-SSFP and single-slice 2D T2-weighted DIR-FSE. Segmented 3D DP-SSFP is a promising sequence for BB CMR of arterial morphology in 3D that warrants further investigation.

## REFERENCES

1. Yuan C, Mitsumori LM, Ferguson MS, Polissar NL, Echelard D, Ortiz G, et al. In vivo accuracy of multispectral magnetic resonance imaging for identifying lipid-rich necrotic cores and intraplaque hemorrhage in advanced human carotid plaques. *Circulation* 2001;104:2051–6.
2. Steinman DA, Rutt BK. On the nature and reduction of plaque-mimicking flow artifacts in black blood MRI of the carotid bifurcation. *Magn Reson Med* 1998;39:635–41.
3. Parker DL, Goodrich KC, Masiker M, Tsuruda JS, Katzman GL. Improved efficiency in double-inversion fast spin-echo imaging. *Magn Reson Med* 2002;47:1017–21.
4. Song HK, Wright AC, Wolf RL, Wehrli FW. Multislice double inversion pulse sequence for efficient black-blood MRI. *Magn Reson Med* 2002;47:616–20.
5. Yarnykh VL, Yuan C. Multislice double inversion-recovery black-blood imaging with simultaneous slice reinversion. *J Magn Reson Imaging* 2003;17:478–483.
6. Mani V, Itskovich VV, Szimtenings M, Aguinaldo JG, Samber DD, Mizsei G, et al. Rapid extended coverage simultaneous

- multisection black-blood vessel wall MR imaging. *Radiology* 2004;232:281–8.
7. Ross R. The pathogenesis of atherosclerosis: a perspective for the 1990s. *Nature* 1993;362:801–9.
  8. Hansson GK. Inflammation, atherosclerosis, and coronary artery disease. *N Engl J Med* 2005;352:1685–95.
  9. Edelman RR, Chien D, Kim D. Fast selective black blood MR imaging. *Radiology* 1991;181:655–60.
  10. Simonetti OP, Finn JP, White RD, Laub G, Henry DA. "Black blood" T2-weighted inversion-recovery MR imaging of the heart. *Radiology* 1996;199:49–57.
  11. Felmlee JP, Ehman RL. Spatial presaturation: a method for suppressing flow artifacts and improving depiction of vascular anatomy in MR imaging. *Radiology* 1987;164:559–64.
  12. Okada Y, Ohtomo K, Kiryu S, Sasaki Y. Breath-hold T2-weighted MRI of hepatic tumors: value of echo planar imaging with diffusion-sensitizing gradient. *J Comput Assist Tomogr* 1998;22:364–71.
  13. Sirol M, Itskovich VV, Mani V, Aguinaldo JG, Fallon JT, Misselwitz B, et al. Lipid-rich atherosclerotic plaques detected by gadofluorine-enhanced in vivo magnetic resonance imaging. *Circulation* 2004;109:2890–6.
  14. Lee H, Price RR. Diffusion imaging with the MP-RAGE sequence. *J Magn Reson Imaging* 1994;4:837–42.
  15. Thomas DL, Pell GS, Lythgoe MF, Gadian DG, Ordidge RJ. A quantitative method for fast diffusion imaging using magnetization-prepared TurboFLASH. *Magn Reson Med* 1998;39:950–60.
  16. Jeong EK, Kim SE, Parker DL. High-resolution diffusion-weighted 3D MRI, using diffusion-weighted driven-equilibrium (DW-DE) and multishot segmented 3D-SSFP without navigator echoes. *Magn Reson Med* 2003;50:821–9.
  17. Numano T, Homma K, Hirose T. Diffusion-weighted three-dimensional MP-RAGE MR imaging. *Magn Reson Imaging* 2005;23:463–8.
  18. Paul D, Hennig J. Comparison of different flip angle variation functions for improved signal behavior in SSFP sequences. *Kyoto, Japan: 2004*; p 2663.
  19. Bogren HG, Klipstein RH, Firmin DN, Mohiaddin RH, Underwood SR, Rees RS, et al. Quantitation of antegrade and retrograde blood flow in the human aorta by magnetic resonance velocity mapping. *Am Heart J* 1989;117:1214–22.
  20. Kilner PJ, Yang GZ, Mohiaddin RH, Firmin DN, Longmore DB. Helical and retrograde secondary flow patterns in the aortic arch studied by three-directional magnetic resonance velocity mapping. *Circulation* 1993;88:2235–47.
  21. Fayad ZA, Nahar T, Fallon JT, Goldman M, Aguinaldo JG, Badimon JJ, et al. In vivo magnetic resonance evaluation of atherosclerotic plaques in the human thoracic aorta: a comparison with transesophageal echocardiography. *Circulation* 2000;101:2503–9.
  22. Mani V, Itskovich VV, Aguiar SH, Mizsei G, Aguinaldo JG, Samber DD, et al. Comparison of gated and non-gated fast multislice black-blood carotid imaging using rapid extended coverage and inflow/outflow saturation techniques. *J Magn Reson Imaging* 2005;22:628–33.
  23. Ku DN, Giddens DP. Pulsatile flow in a model carotid bifurcation. *Arteriosclerosis* 1983;3:31–9.
  24. Motomiya M, Karino T. Flow patterns in the human carotid artery bifurcation. *Stroke* 1984;15:50–6.
  25. Luk-Pat GT, Gold GE, Olcott EW, Hu BS, Nishimura DG. High-resolution three-dimensional in vivo imaging of atherosclerotic plaque. *Magn Reson Med* 1999;42:762–71.
  26. Bland JM, Altman DG. Statistical methods for assessing agreement between two methods of clinical measurement. *Lancet* 1986;1:307–10.
  27. Constable RT, Gore JC. The loss of small objects in variable TE imaging: implications for FSE, RARE, and EPI. *Magn Reson Med* 1992;28:9–24.
  28. Garcia JH, Khang-Loon H. Carotid atherosclerosis. Definition, pathogenesis, and clinical significance. *Neuroimaging Clin N Am* 1996;6:801–10.
  29. Tunick PA, Kronzon I. Atheromas of the thoracic aorta: clinical and therapeutic update. *J Am Coll Cardiol* 2000;35:545–54.
  30. Kallikazaros IE, Tsioufis CP, Stefanadis CI, Pitsavos CE, Toutouzas PK. Closed relation between carotid and ascending aortic atherosclerosis in cardiac patients. *Circulation* 2000;102:III263–8.
  31. Jaffer FA, O'Donnell CJ, Larson MG, Chan SK, Kissinger KV, Kupka MJ, et al. Age and sex distribution of subclinical aortic atherosclerosis: a magnetic resonance imaging examination of the Framingham Heart Study. *Arterioscler Thromb Vasc Biol* 2002;22:849–54.
  32. Taniguchi H, Momiyama Y, Fayad ZA, Ohmori R, Ashida K, Kihara T, et al. In vivo magnetic resonance evaluation of associations between aortic atherosclerosis and both risk factors and coronary artery disease in patients referred for coronary angiography. *Am Heart J* 2004;148:137–43.
  33. Yonemura A, Momiyama Y, Fayad ZA, Ayaori M, Ohmori R, Higashi K, et al. Effect of lipid-lowering therapy with atorvastatin on atherosclerotic aortic plaques detected by noninvasive magnetic resonance imaging. *J Am Coll Cardiol* 2005;45:733–42.
  34. Dart AM, Lacombe F, Yeoh JK, Cameron JD, Jennings GL, Laufer E, et al. Aortic distensibility in patients with isolated hypercholesterolaemia, coronary artery disease, or cardiac transplant. *Lancet* 1991;338:270–3.
  35. van Popele NM, Grobbee DE, Bots ML, Asmar R, Topouchian J, Reneman RS, et al. Association between arterial stiffness and atherosclerosis: the Rotterdam Study. *Stroke* 2001;32:454–60.
  36. Bogren HG, Buonocore MH. 4D magnetic resonance velocity mapping of blood flow patterns in the aorta in young vs. elderly normal subjects. *J Magn Reson Imaging* 1999;10:861–9.
  37. Hunink MG, Polak JF, Barlan MM, O'Leary DH. Detection and quantification of carotid artery stenosis: efficacy of various Doppler velocity parameters. *Am J Roentgenol* 1993;160:619–25.